JMEPEG (2019) 28:2747–2753
https://doi.org/10.1007/s11665-019-04093-0

1059-9495/$19.00

Fabrication and Characterization of A5083-WC-Al_2O_3 Surface Composite by Friction Stir Processing

Akbar Heidarpour

(Submitted January 16, 2019; in revised form April 14, 2019; published online May 9, 2019)

In this study, WC-Al_2O_3 ceramic composite was incorporated into Al5083 to produce a surface composite by friction stir processing (FSP), and the microstructure, hardness and wear properties of Al5083-WC-Al_2O_3 surface composite were evaluated. Optical microscopy of FSPed samples showed grain refinement in the stir zone. The addition of WC-Al_2O_3 particles as well as increase in FSP pass number had a considerable effect on grain refinement, and the grain size of Al5083 base metal of 36 µm reduced to 11 µm for Al5083-WC-Al_2O_3 surface composite after four passes. The SEM observation of the surface composite revealed that the WC-Al_2O_3 particles distributed homogenously in the matrix and by increasing the FSP passes, the initial agglomerates of mechanochemically synthesized WC-Al_2O_3 powders could be fractured. Microhardness evaluation showed a substantial improvement by adding WC-Al_2O_3 particles and increase in FSP pass number. The maximum microhardness value of 101 HV belonged to surface composite after four passes, while the microhardness of the base metal was 65 HV. Wear test results revealed enhanced tribological behavior with a similar trend of microhardness values. Scanning electron microscopy tests revealed both adhesive and abrasive wear mechanisms on the surface of the wear test specimens.

Keywords aluminum alloy, friction stir processing, microstructure, microhardness, wear, WC-Al_2O_3 particles

1. Introduction

Aluminum alloys are one of the important lightweight materials and were chosen for broad structural applications (Ref 1, 2). Generally, the wear resistance of these alloys is poor and limits their application. Several approaches suggested overcoming this limitation. Fabricating a surface composite is a good solution to harden the surface and enhance the wear resistance (Ref 3). Several methods are introduced for fabricating the surface composite such as TIG cladding processes (Ref 4-6), laser cladding (Ref 7), applying a composite layer by thermal spraying methods (Ref 8-10) and friction stir processing (FSP) (Ref 11, 12). In spite of the FSP, almost processing techniques are ordinarily performed at high temperatures and in the liquid phase. In this situation, several problems associated with liquid phases such as unwanted reaction at the interface of reinforcement and the matrix, and harmful phase transformation could occur. Moreover, to achieve desirable microstructure on the surface, crucial control of processing parameters is necessary. Clearly, if the surface treatment is performed in the solid state, the above-mentioned problems may be diminished. FSP is a solid-state processing technique and an effective method for fabricating the surface composites (Ref 12-17). The FSP was successful in producing surface composites without limitation of the liquid phase and high-temperature effects. A significant development in the microstructure has occurred during the FSP because a severe plastic deformation occurred and the substance undergoes a thermal exposure (Ref 18). As a result, three distinct microstructural zones are created: the heat affected zone (HAZ), the thermomechanically affected zone (TMAZ) and the stir zone (SZ). Because of severe plastic deformation, fine grains can be achieved in the stir zone. In other words, the microstructure of the stir zone is mainly composed of equiaxed grains because of dynamic recrystallization (Ref 19-21).

A growing body of literature has investigated the effect of FSP on mechanical and tribological properties of the various metals, especially aluminum. Most studies have focused on the positive impact of these methods on properties of the metals reported (Ref 22-24). Before investigating Al5083 surface composites, it should be mentioned that Al 5083 is one of the important aluminum alloys that inherited several good properties such as good strength, weldability and corrosion resistance. Fabrication of a surface composite on 5083 aluminum is a good way to improve the surface hardness and enhance tribological behavior. Until now, Al 5083 was used to fabricate surface composite by adding different reinforcements including ZrO_2 (Ref 25), CNT (carbon nanotube) and CeO_2 (Ref 26, 27), W (Ref 28, 29), Ni (Ref 30), SiC (Ref 31), Al_2O_3 and TiO_2 (Ref 32), etc.

Recently, Al_2O_3 and TiO_2 particles were successfully incorporated into 5083 Al alloy and enhanced mechanical and tribological properties were reported (Ref 22, 32). In these studies, the hybrid ratio of Al_2O_3 and TiO_2 particles and rotational and travel speed were examined to find optimum conditions. To the best of the authors' knowledge, there are not any previous study on fabrication and characterization of Al5083-WC-Al_2O_3 surface composite by FSP. In this study, WC-Al_2O_3 composite was used to process Al5083-WC-Al_2O_3 surface composite via FSP. The effect of particle addition on the microstructure, hardness and the wear behavior was investigated.

Akbar Heidarpour, Department of Metallurgy and Materials Engineering, Hamedan University of Technology, Hamedan 65155-579, Iran. Contact e-mail: a.heidarpour@gmail.com.

Table 1 Chemical composition of Al5083 bars

Substance	Al	Mg	Si	Fe	Cu	Mn	Zn	Ti
wt.%	Bal.	4.27	0.1	0.31	0.04	0.61	0.02	0.02

2. Experimental

In this study, an Al5083 sheet of 5 mm thickness in the annealed condition, with the chemical analysis given in Table 1, was cut in bars of 140 mm × 50 mm × 5 mm for the FSP experiments. A mixture of WC-Al_2O_3 powders was used as reinforcement, and the synthesis of these powders was described elsewhere (Ref 33). The particle size of these powders was in the range of 0.5-1 μm, and an SEM micrograph is exhibited in Fig. 1.

An FSP machine was equipped with a fixture in order to apply the process on the samples. The fixtures were designed in a way to keep specimens firm on the machine and prevent sample movement when the process was carried out. To insert the powder into the matrix, a groove of l mm × 2 mm was created on the base metal and then was filled with the WC-Al_2O_3 powders. For FSP, at first and after filling the groove with reinforcements, a pin-less tool was used to close the groove. This guarantees powder packing and avoids powder spreading. Then, FSP was conducted by a tool with a square pin. Both tools are made of hot working steel, and the shoulders diameter was 20 mm. The square pin has the dimensions of 6 × 6 mm and a length of 3 mm. In order to obtain sound specimen without flaws and to have the most properties, several combinations of speeds, both rotational and transverse, were tested. According to the results, the optimum sample was obtained for the tool rotational and transverse speeds of 900 rpm and 63 mm/min, respectively. Then, these speeds were chosen to process all samples. Also, the rotation direction of the FSP tool was in the clockwise direction with a tilt angle of 3 degrees. The four-pass FSP, all traversed in opposite directions alternately. According to the above-mentioned procedure, several samples were processed, and the sample codes are given in Table 2.

The optical microstructure of the FSPed samples was collected by an optical microscope of Dewinter DMI equipped with a digital optical scanner. The composition of etchant, used in this study, consisted of 2 ml HF, 3 ml HCl, 20 ml HNO_3 and 175 ml distilled water (Keller's regent). The microstructural characterization and elemental composition of the friction stirred samples were analyzed using a scanning electron microscope (FEI ESEM QUANTA 200) equipped with an energy-dispersive spectrometer (EDS). In addition, grain size measurement was carried out using an image analyzer. The Vickers microhardness test was performed by Buhler's equipment with a load of 200 g for 15 s. Both microstructural observation and microhardness profile were taken from the cross section of FSPed samples.

To examine the tribological behavior of Al5083 base metal and FSPed samples, pin-on-disk wear test was conducted on the samples by a tribometer (DUCOM) according to ASTM G99-04 standard. In this test, the pin was made of FSPed samples, and the disk was made of EN-24 steel hardened to 58 HRC. Sliding speed was 0.3 m/s and kept constant during the test, and the normal loads of 10 N were used. The sliding distance was 500 m for all the samples. Before and after testing, the pin and disk were cleaned with acetone and were weighed with an electronic weighing balance with an accuracy of 0.1 mg to calculate wear rate. In addition to wearing rate, the coefficient of friction during the test was measured using frictional force and applied load. SEM was used to explore the worn surface to deduce the wear mechanisms.

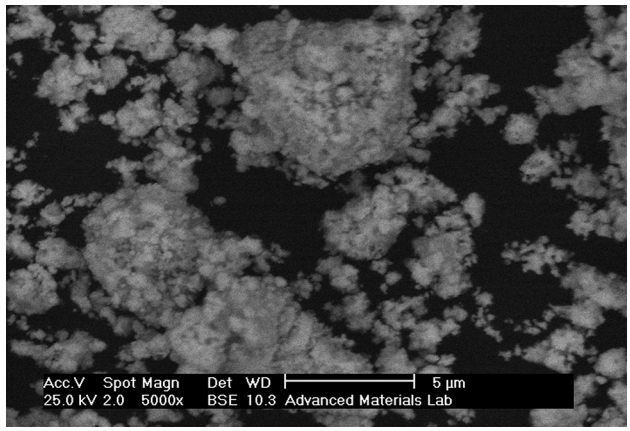

Fig. 1 Backscattered SEM micrographs of the WC-Al_2O_3 powders

Table 2 Code of samples

Sample	Code
As-received Al5083	BM
Al5083 after one-pass FSP without reinforcement	FSPed BM
Al5083 after one-pass FSP with WC-Al_2O_3 powders	1P
Al5083 after four-pass FSP with WC-Al_2O_3 powders	4P

3. Results and Discussion

3.1 Microstructural Characterization

The structure of the BM, FSPed BM, 1P and 2P specimens of the stir zone (SZ) is shown in Fig. 2. All micrographs consist of equiaxed fine grains, and no defects including voids or cracks were seen in the stir zone of samples.

A comparison between the grain size of shown BM and SZ zones reveals that a grain size refining has occurred for FSPed samples. It is obvious that the use of FSP has led to the proper grain refinement of Al5083 for all the samples. It is worth noting that the grain refinement of aluminum is caused by dynamic recrystallization during FSP. During FSP, because of high stacking fault energy of aluminum alloys, dislocations can easily glide/climb through dynamic recovery (DRV). Also, it could be said that the continuous dynamic recrystallization (CDRX) is a possible recrystallization mechanism for aluminum alloys, during FSP (Ref 34).

The grain sizes of SZ for BM, FSPed BM, 1P and 4P specimens obtained were 36, 28, 18 and 11 μm, respectively. Clearly, the addition of WC-Al_2O_3 particles as well as increasing pass number had a considerable effect on grain refinement. A significant change in the grain size of the stir

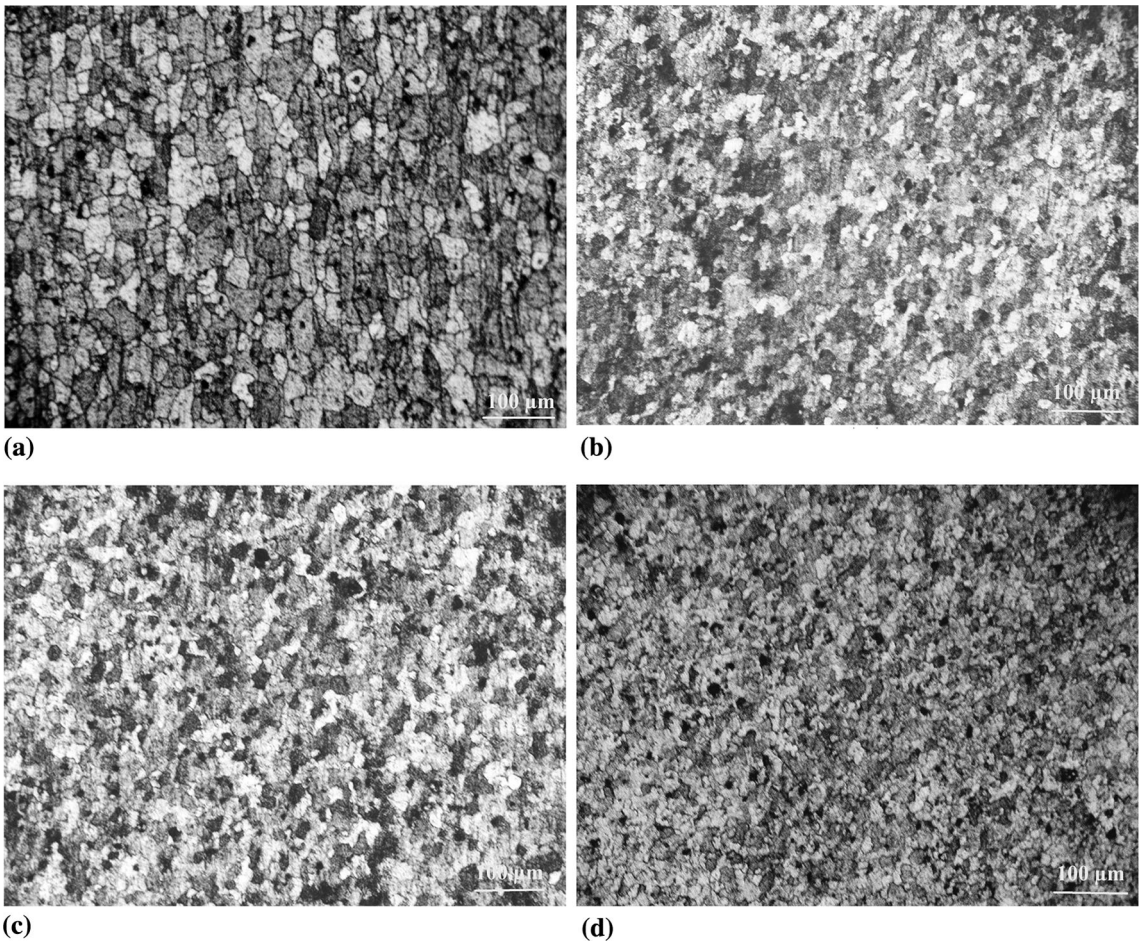

Fig. 2 Optical images of (a) BM, (b) FSPed BM, (c) 1P and (d) 4P specimens

zone occurred due to the friction process and the numerous plastic deformations during FSP. The factors controlling the size of the grain in the stir zone are (Ref 16, 35, 36): 1—dynamic recrystallization because of continuous plastic deformation and severe dynamic stress in the stir zone and 2—the presence of WC-Al_2O_3 particles creates a pinning state in the stir zone, which prevents the growth and movement of the grains. These reasons have a significant effect on grain growth control.

Figure 3 shows the SEM micrograph of stir zone of the 1P and 4P specimens. SEM micrograph of the 1P specimen (Fig. 3a) reveals a non-uniform distribution of reinforcements. Since the WC-Al_2O_3 particles were synthesized by mechanical milling of elemental primary powders (Ref 33), it consisted of very small and agglomerated particles, as seen in Fig. 1. After one pass of FSP, these particles were distributed in the Al5083 matrix. Uniform dispersion of the particles mainly depended on materials flow during FSP. By increasing the pass numbers of FSP, the uniform dispersion of the particles was improved, and a uniform and homogeneous distribution of the WC-Al_2O_3 particles is clearly observed in Fig. 3(b). Actually, the FSP could fracture the agglomerates of initial powders and disperse within the matrix. Figure 4 shows an elemental composition mapping of the 4P specimen. The white particles are WC while the gray particles are Al_2O_3, and WC particle contains some Al_2O_3.

3.2 Microhardness

The microhardness profiles of BM and FSPed specimens are illustrated in Fig. 5. The mean microhardness value of Al5083 was found to be 65 HV. There are significant changes in the hardness value after FSP. The average microhardness values are presented in Table 3. Microhardness of Al5083 base metal increased about 9% after FSP without addition reinforcements (FSPed BM). But, by adding WC-Al_2O_3 particles, microhardness improved (1P) and this value increased to 81 HV. Further increase in microhardness value of 101 HV occurred after four passes (4P), which is related to about 55% enhancement in microhardness than base metal. It could be concluded that the FSP without addition of WC-Al_2O_3 particles has limited effect on microhardness enhancement of Al5083, whereas a significant increase in microhardness was observed in the presence of reinforcements which shifts microhardness curve up and maximum microhardness was measured for the 4P specimen.

In fact, it is well established that the incorporation of a second phase, e.g., WC-Al_2O_3, in the aluminum matrix causes increase in the strength values via several mechanisms such as pinning effect (Ref 22, 37, 38), Orowan mechanism (Ref 12, 39), as well as the mismatch of the coefficients of thermal expansion (CTE) (Ref 40, 41). Accordingly, it can be deduced that for the 4P specimen, the strengthening mechanisms have a

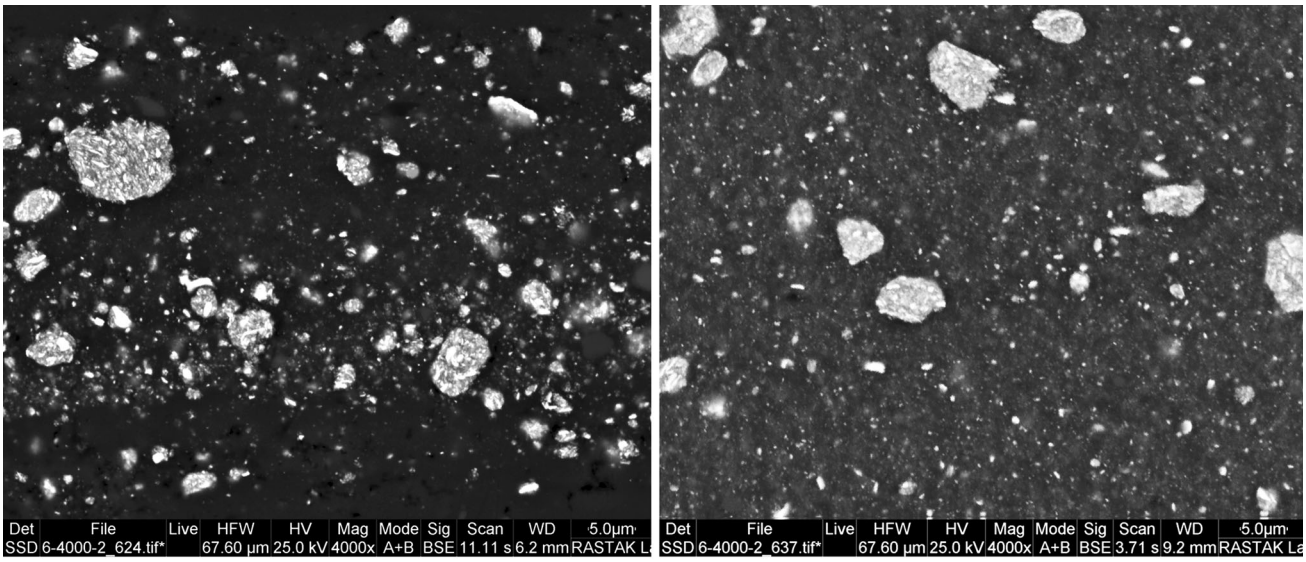

Fig. 3 SEM micrograph of (a) 1P and (b) 4P specimens

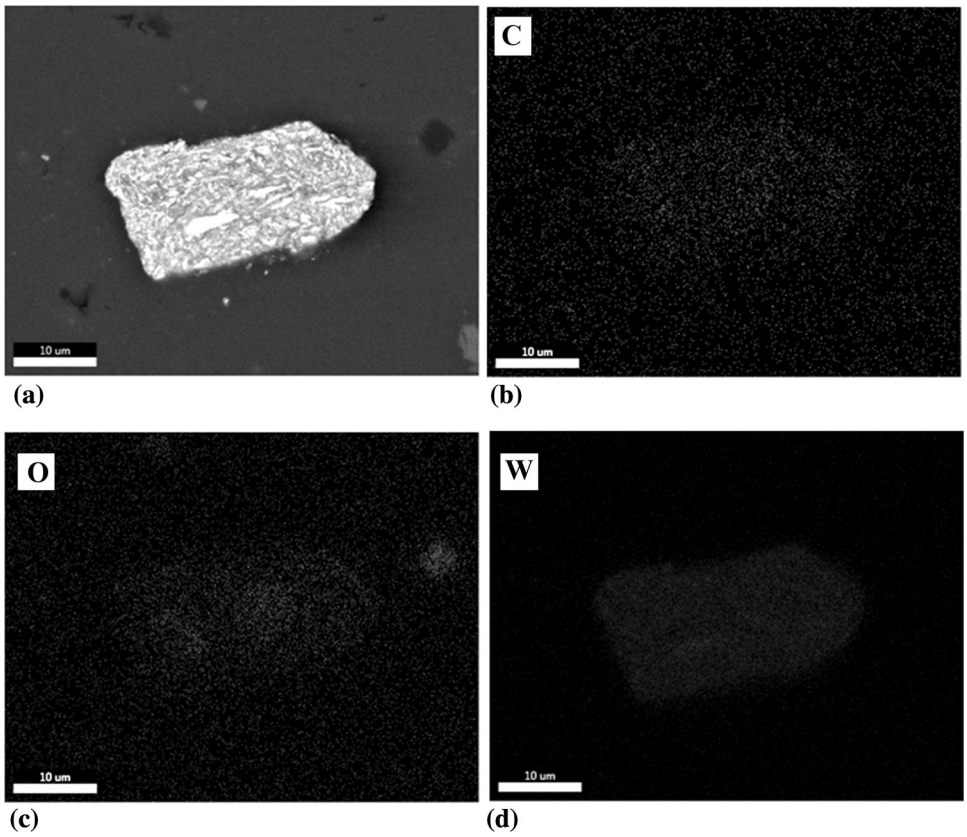

Fig. 4 (a) Cross-sectional SEM micrograph of stir zone of the 4P specimen, and the elemental mapping of (b) carbon, (c) oxygen and (d) tungsten

stronger role in mechanical properties and this sample had maximum microhardness value. In contrast to the 1P specimen which had a slight increase in microhardness value, the proper mixing and sufficient materials flow after four passes enhanced homogenous dispersion of the second phase and then its impact.

3.3 Wear Behavior

Figure 6 shows the weight loss as a function of sliding distance for BM, FSPed BM, 1P and 4P specimens. Obviously, the wear rate is considerably decreased when the FSP is applied on the surface of Al5083 and by addition WC-Al_2O_3 particles and even by increasing passes of FSP up to 4. Thus, the

minimum weight loss belongs to the 4P sample. The wear rates for Al5083 base metal and FSPed specimens are presented in Table 3. Here, a similar trend is observed, and this behavior can be ascribed to the higher hardness of the 4P specimen.

There is a reverse relation between hardness and the wear rate, named as Archard's equation (Ref 24, 32). According to Table 3, the reverse relationship between hardness and the wear rate is seen. The WC-Al_2O_3 particles are hard particles and resist the penetration and cutting into the surface by the counter material. It can be concluded from these results that the wear resistance of the surface composite significantly was enhanced by the friction stir processing due to the intensive grain refinement during the process (Ref 23, 42, 43).

Figure 7 shows the variations in the friction coefficient of the BM, FSPed BM, 1P and 4P samples as a function of sliding distance. The average friction coefficient values are presented in Table 3. As it could be seen, the maximum friction coefficient was related to the BM of 0.54, and the lowest was obtained for four-pass FSPed specimen of 0.16. As the number of passes increases, the friction coefficient decreases. This sample, 4P, as mentioned above, has a maximum microhardness value, lowest wear rate and here, minimum friction coefficient.

In all curves of Fig. 7, some fluctuations in the friction coefficient are observed. This may be attributed to the periodical accumulation and elimination of wear debris on the worn track. Moreover, the repeated banding structure in the tool traveling direction resulting from the tool pitch, which was considered one of the significant characteristics of FSW/FSP, may contribute to this fluctuation (Ref 44).

To examine the wear mechanism, the surface morphology of the worn specimen was analyzed by SEM. Figure 8 shows SEM micrographs of BM, FSPed BM, 1P and 4P worn surfaces. Figure 8(a) shows pits and deep grooves which prove adhesive wear in wear surface morphology of base metal. It reveals that intensive material removal and plastic deformation have occurred. Wider and deeper grooves in the worn surface of this specimen indicate that adhesive wear has happened (Ref 24). After FSP of base metal (FSPed BM specimen), and as seen from Fig. 8(b), the pits and grooves decreased due to a higher hardness than base metal. The presence of reinforcing particles in FSPed specimens with WC-Al_2O_3 particles pre-

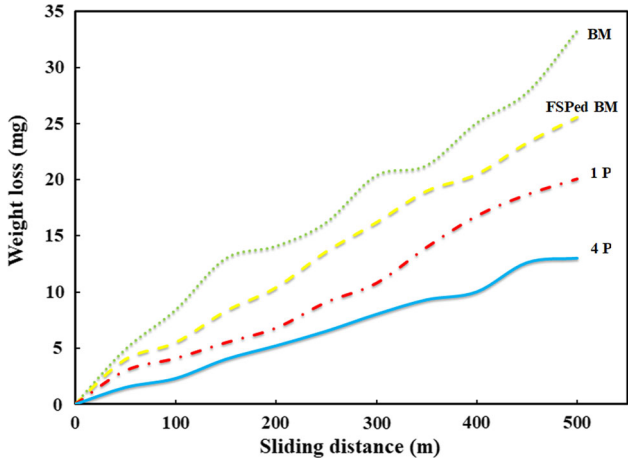

Fig. 6 Variation of weight loss of BM, FSP-BM, 1P and 4P specimens as a function of sliding distance

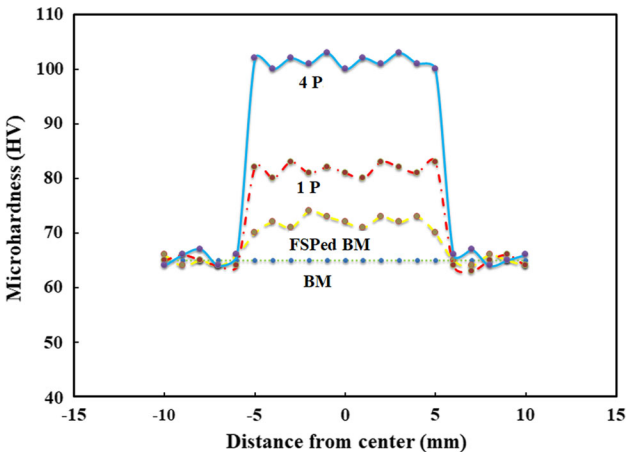

Fig. 5 Cross-sectional microhardness profiles of samples

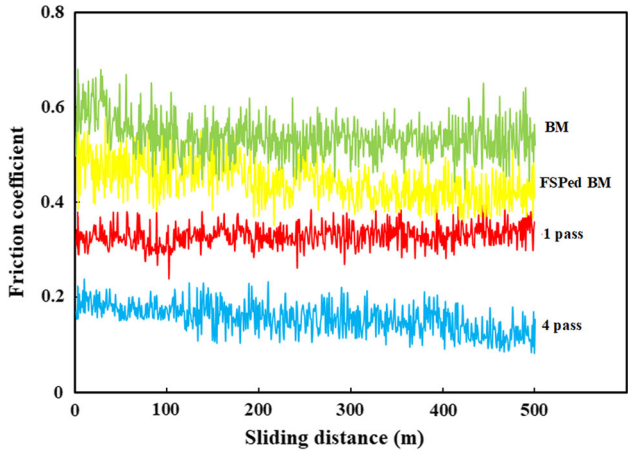

Fig. 7 Variation of the friction coefficient of BM, FSPed BM, 1P and 4P specimens as a function of sliding distance

Table 3 Average of grain size, microhardness, wear rate and friction coefficient of samples

Sample	Size (μm) ± 2	Microhardness	Wear rate, mg/m	Friction coefficient
BM	36	65	0.07	0.54
FSP-BM	28	72	0.057	0.45
1P	18	82	0.04	0.33
4P	11	101	0.026	0.16

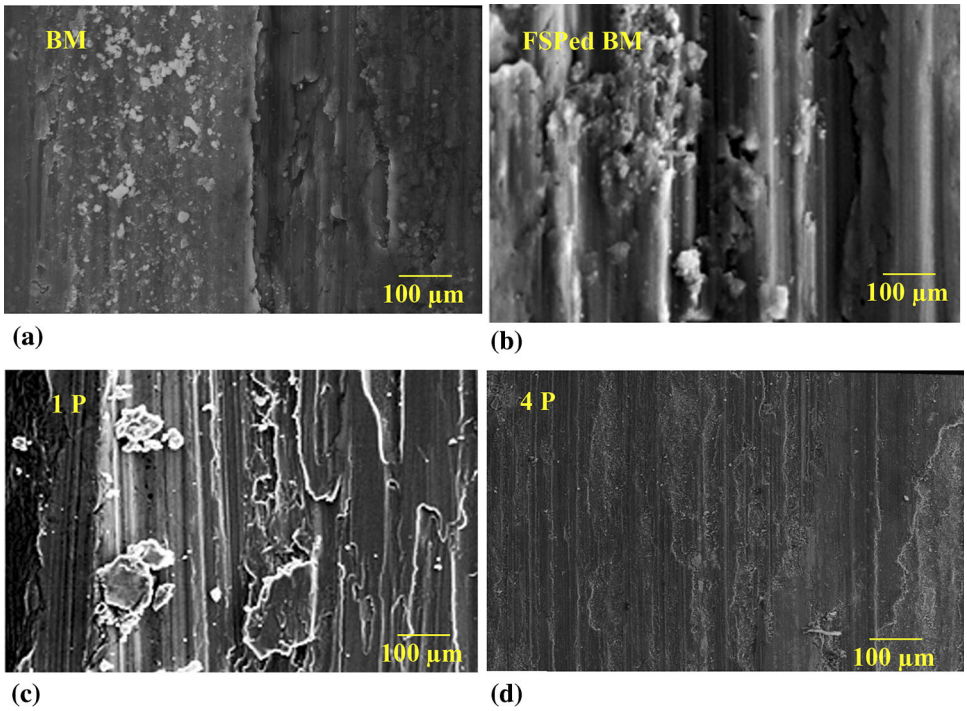

Fig. 8 SEM micrographs of worn surfaces of base metal and FSPed specimens

vents adhesive wearing and drastic material removal. The SEM micrographs of the surface composites, i.e., the 1P and 4P specimens, represent many parallel grooves in the smooth worn surface, and materials piled up at the edge of grooves and partly broke. Piled-up and partly broken materials at the edge of grooves are evidence indicating metal flow and crater, as well as micro-cracks on the FSPed worn surfaces. The evidence indicating both adhesive and abrasive wear mechanisms in other samples has been observed. The metal removal rate during sliding is less in abrasive mode compared to the adhesive mode of wear. Therefore, it can be concluded that the as-received base metal and FSPed BM have adhesive wear mechanism, and surface composites have both adhesive and abrasive wear mechanisms. According to the wear rate (Fig. 6 and Table 2), abrasive wear is the dominant wear mechanism in specimens equipped with the surface composite layer.

4. Conclusion

Fabrication of WC-Al_2O_3-reinforced Al5083 surface composite by FSP was successful. Microstructural investigation showed that FSP causes grain refinement and by adding WC-Al_2O_3 particles, this refinement intensifies and after four-pass FSP, the grain size reduced to 11 µm. The SEM results showed that WC-Al_2O_3 particles were dispersed regularly in the Al5083 with a small quantity of clusters or agglomerates after four-pass FSP. Results of hardness test showed that FSP without addition of WC-Al_2O_3 particles (FSPed BM) had a little impact on the hardness value, while the addition of WC-Al_2O_3 particles, as well as increasing pass number, had a significant impact on hardness value due to more grain refinement and effective dispersion of reinforcements. Surface composites revealed lower friction coefficients and wear rates, which were significantly lower than those obtained for the base metal. Scanning electron microscopy tests revealed both adhesive and abrasive wear mechanisms on the surface of the wear test specimens.

References

1. I. Polmear, D.S. John, J.F. Nie, and M. Qian, *Light Alloys: Metallurgy of the Light Metals*, 5th ed., Butterworth-Heinemann, Chennai, 2017
2. F.C. Campbell, Manufacturing Technology for Aerospace Structural Materials, *Manuf. Technol. Aerosp. Struct. Mater.*, 2006, https://doi.org/10.1016/b978-185617495-4/50002-0
3. M. Akbari, M.H. Shojaeefard, P. Asadi, and A. Khalkhali, Wear and Mechanical Properties of Surface Hybrid Metal Matrix Composites on Al-Si Aluminum Alloys Fabricated by Friction Stir Processing, *Proc. Inst. Mech. Eng. Part L J. Mater. Des. Appl.*, 2017, **233**, p 790–799. https://doi.org/10.1177/1464420717702413
4. M. Tavoosi, S. Arjmand, and B. Adelimoghaddam, Surface Alloying of Commercially Pure Titanium with Aluminium and Nitrogen Using GTAW Processing, *Surf. Coat. Technol.*, 2017, **311**, p 314–320. https://doi.org/10.1016/j.surfcoat.2016.12.115
5. M. Tavoosi and S. Arjmand, In Situ Formation of Al/Al_3Ti Composite Coating on Pure Ti Surface by TIG Surfacing Process, *Surf. Interfaces*, 2017, **8**, p 1–7. https://doi.org/10.1016/j.surfin.2017.04.002
6. F. Ghadami, M. Heydarzadeh Sohi, and S. Ghadami, Effect of TIG Surface Melting on Structure and Wear Properties of Air Plasma-Sprayed WC-Co Coatings, *Surf. Coat. Technol.*, 2015, **261**, p 108–113. https://doi.org/10.1016/j.surfcoat.2014.11.050
7. V. Kishan, A. Devaraju, and K.P. Lakshmi, Tribological Properties of Nano TiB_2 Particle Reinforced 6061-T6 Aluminum Alloy Surface Composites via Friction Stir Processing, *Mater. Today Proc.*, 2018, **5**(1, Part 1), p 1615–1619. https://doi.org/10.1016/j.matpr.2017.11.254
8. K.A. Habib, J.J. Saura, C. Ferrer, M.S. Damra, E. Giménez, and L. Cabedo, Comparison of Flame Sprayed Al_2O_3/TiO_2 Coatings: Their Microstructure, Mechanical Properties and Tribology Behavior, *Surf. Coat. Technol.*, 2006, **201**(3-4), p 1436–1443
9. D. Chaliampalias, S. Andronis, N. Pliatsikas, E. Pavlidou, D. Tsipas, S. Skolianos, K. Chrissafis, G. Stergioudis, P. Patsalas, and G. Vourlias, Formation and Oxidation Resistance of Al/Ni Coatings on Low Carbon Steel by Flame Spray, *Surf. Coat. Technol.*, 2014, **255**, p 62–68

10. N. Kahraman and B. Gülenç, Abrasive Wear Behaviour of Powder Flame Sprayed Coatings on Steel Substrates, *Mater. Des.*, 2002, **23**(8), p 721–725. https://doi.org/10.1016/S0261-3069(02)00075-4
11. A. Kurt, I. Uygur, and E. Cete, Surface Modification of Aluminium by Friction Stir Processing, *J. Mater. Process. Technol.*, 2011, **211**(3), p 313–317. https://doi.org/10.1016/j.jmatprotec.2010.09.020
12. H.S. Arora, H. Singh, and B.K. Dhindaw, Composite Fabrication Using Friction Stir Processing—A Review, *Int. J. Adv. Manuf. Technol.*, 2012, **61**(9–12), p 1043–1055
13. R.S. Mishra and Z.Y. Ma, Friction Stir Welding and Processing, *Mater. Sci. Eng. R Rep.*, 2005, **50**, p 1–78. https://doi.org/10.1016/j.mser.2005.07.001
14. V.K.S. Jain, P.M. Muhammed, S. Muthukumaran, and S.P.K. Babu, Microstructure, Mechanical and Sliding Wear Behavior of AA5083-B_4C/SiC/TiC Surface Composites Fabricated Using Friction Stir Processing, *Trans. Indian Inst. Met.*, 2018, **71**(6), p 1519–1529. https://doi.org/10.1007/s12666-018-1287-y
15. N. Yuvaraj and S. Aravindan, Wear Characteristics of Al5083 Surface Hybrid Nano-Composites by Friction Stir Processing, *Trans. Indian Inst. Met.*, 2017, **70**(4), p 1111–1129
16. D. Yadav and R. Bauri, Friction Stir Processing of Al-TiB_2 In Situ Composite: Effect on Particle Distribution, Microstructure and Properties, *J. Mater. Eng. Perform.*, 2015, **24**(3), p 1116–1124. https://doi.org/10.1007/s11665-015-1404-6
17. H.C. Madhu, P. Ajay Kumar, C.S. Perugu, and S.V. Kailas, Microstructure and Mechanical Properties of Friction Stir Process Derived Al-TiO_2 Nanocomposite, *J. Mater. Eng. Perform.*, 2018, https://doi.org/10.1007/s11665-018-3188-y
18. G.K. Padhy, C.S. Wu, and S. Gao, Friction Stir Based Welding and Processing Technologies-Processes, Parameters, Microstructures and Applications: A Review, *J. Mater. Sci. Technol.*, 2018, **34**, p 1–38
19. F. Humphreys and M. Matherly, *Recrystallization and Related Annealing Phenomena*, 2nd ed., Elsevier, New York, 1995, p 173–178
20. F.J. Humphreys, P.B. Prangnell, and R. Priestner, Fine-Grained Alloys by Thermomechanical Processing, *Curr. Opin. Solid State Mater. Sci.*, 2001, **5**(1), p 15–21
21. S. Swaminathan, K. Oh-Ishi, A.P. Zhilyaev, C.B. Fuller, B. London, M.W. Mahoney, and T.R. McNelley, Peak Stir Zone Temperatures during Friction Stir Processing, *Metall. Mater. Trans. A Phys. Metall. Mater. Sci.*, 2010, **41**(3), p 631–640
22. S. Ahmadifard, S. Kazemi, and A. Heidarpour, Production and Characterization of A5083-Al_2O_3-TiO_2 Hybrid Surface Nanocomposite by Friction Stir Processing, *Proc. Inst. Mech. Eng. Part L J. Mater. Des. Appl.*, 2018, **232**(4), p 287–293. https://doi.org/10.1177/1464420715623977
23. N. Yuvaraj and S. Aravindan, Fabrication of Al5083/B_4C Surface Composite by Friction Stir Processing and Its Tribological Characterization, *J. Mater. Res. Technol.*, 2015, **4**(4), p 398–410. https://doi.org/10.1016/j.jmrt.2015.02.006
24. Y. Mazaheri, F. Karimzadeh, and M.H. Enayati, Tribological Behavior of A356/Al_2O_3 Surface Nanocomposite Prepared by Friction Stir Processing, *Metall. Mater. Trans. A*, 2014, **45**(4), p 2250–2259. https://doi.org/10.1007/s11661-013-2140-x
25. S. Shahraki, S. Khorasani, R. Abdi Behnagh, Y. Fotouhi, and H. Bisadi, Producing of AA5083/ZrO_2 Nanocomposite by Friction Stir Processing (FSP), *Metall. Mater. Trans. B*, 2013, **44**(6), p 1546–1553. https://doi.org/10.1007/s11663-013-9914-9
26. S.A. Hosseini, K. Ranjbar, R. Dehmolaei, and A.R. Amirani, Fabrication of Al5083 Surface Composites Reinforced by CNTs and Cerium Oxide Nano Particles via Friction Stir Processing, *J. Alloys Compd.*, 2015, **622**, p 725–733. https://doi.org/10.1016/j.jallcom.2014.10.158
27. M. Amra, K. Ranjbar, and R. Dehmolaei, Mechanical Properties and Corrosion Behavior of CeO_2 and SiC Incorporated Al5083 Alloy Surface Composites, *J. Mater. Eng. Perform.*, 2015, **24**(8), p 3169–3179
28. C.N. Shyam Kumar, R. Bauri, and D. Yadav, Wear Properties of 5083 Al-W Surface Composite Fabricated by Friction Stir Processing, *Tribol. Int.*, 2016, **101**, p 284–290. https://doi.org/10.1016/j.triboint.2016.04.033
29. R. Bauri, D. Yadav, C.N. Shyam Kumar, and B. Balaji, Tungsten Particle Reinforced Al 5083 Composite with High Strength and Ductility, *Mater. Sci. Eng. A*, 2014, **620**, p 67–75. https://doi.org/10.1016/j.msea.2014.09.108
30. R. Bauri, G.D. Janaki Ram, D. Yadav, and C.N. Shyam Kumar, Effect of Process Parameters and Tool Geometry on Fabrication of Ni Particles Reinforced 5083 Al Composite by Friction Stir Processing, *Mater. Today Proc.*, 2015, **2**(4-5), p 3203–3211. https://doi.org/10.1016/j.matpr.2015.07.115
31. H.I. Kurt, Influence of Hybrid Ratio and Friction Stir Processing Parameters on Ultimate Tensile Strength of 5083 Aluminum Matrix Hybrid Composites, *Compos. Part B Eng.*, 2016, **93**, p 26–34. https://doi.org/10.1016/j.compositesb.2016.02.056
32. A. Heidarpour, S. Ahmadifard, and S. Kazemi, On the Al5083-Al_2O_3-TiO_2 Hybrid Surface Nanocomposite Produced by Friction Stir Processing, *Prot. Met. Phys. Chem. Surf.*, 2018, **54**(3), p 409–415. https://doi.org/10.1134/S2070205118030279
33. A. Heidarpour, N. Shahin, and S. Kazemi, A Novel Approach to in Situ Synthesis of WC-Al_2O_3 Composite by High Energy Reactive Milling, *Int. J. Refract. Met. Hard Mater.*, 2017, **64**, p 1–6
34. T.R. McNelley, Friction Stir Processing (FSP): Refining Microstructures and Improving Properties, *Rev. Metal.*, 2010, **46**, p 149–156. https://doi.org/10.3989/revmetalmadrid.19XIIPMS
35. R. Abdi Behnagh, M.K. Besharati Givi, and M. Akbari, Mechanical Properties, Corrosion Resistance, and Microstructural Changes during Friction Stir Processing of 5083 Aluminum Rolled Plates, *Mater. Manuf. Process.*, 2012, **27**(6), p 636–640
36. Y. Chen, H. Ding, J. Li, Z. Cai, J. Zhao, and W. Yang, Influence of Multi-Pass Friction Stir Processing on the Microstructure and Mechanical Properties of Al-5083 Alloy, *Mater. Sci. Eng. A*, 2016, **650**, p 281–289. https://doi.org/10.1016/j.msea.2015.10.057
37. J.F. Guo, J. Liu, C.N. Sun, S. Maleksaeedi, G. Bi, M.J. Tan, and J. Wei, Effects of Nano-Al_2O_3 Particle Addition on Grain Structure Evolution and Mechanical Behaviour of Friction-Stir-Processed Al, *Mater. Sci. Eng. A*, 2014, **602**, p 143–149. https://doi.org/10.1016/j.msea.2014.02.022
38. I.S. Lee, C.J. Hsu, C.F. Chen, N.J. Ho, and P.W. Kao, Particle-Reinforced Aluminum Matrix Composites Produced from Powder Mixtures via Friction Stir Processing, *Compos. Sci. Technol.*, 2011, **71**(5), p 693–698
39. R. Yang, Z. Zhang, Y. Zhao, G. Chen, Y. Guo, M. Liu, and J. Zhang, Effect of Multi-Pass Friction Stir Processing on Microstructure and Mechanical Properties of Al_3Ti/A356 Composites, *Mater. Charact.*, 2015, **106**, p 62–69. https://doi.org/10.1016/j.matchar.2015.05.019
40. K.-M. Lee, D.-K. Oh, W.-S. Choi, T. Weissgärber, and B. Kieback, Thermomechanical Properties of AlN-Cu Composite Materials Prepared by Solid State Processing, *J. Alloys Compd.*, 2007, **434-435**, p 375–377. https://doi.org/10.1016/j.jallcom.2006.08.176
41. S. Rathee, S. Maheshwari, and A.N. Siddiquee, Issues and Strategies in Composite Fabrication via Friction Stir Processing: A Review, *Mater. Manuf. Process.*, 2018, **33**, p 239–261
42. R.S. Mishra, Z.Y. Ma, and I. Charit, Friction Stir Processing: A Novel Technique for Fabrication of Surface Composite, *Mater. Sci. Eng. A*, 2003, **341**(5), p 307–310
43. N. Yuvaraj and S. Aravindan, Comparison Studies on Mechanical and Wear Behavior of Fabricated Aluminum Surface Nano Composites by Fusion and Solid State Processing, *Surf. Coat. Technol.*, 2017, **309**, p 309–319. https://doi.org/10.1016/j.surfcoat.2016.11.076
44. T.S. Mahmoud, O.M. Shaban, H.M. Zakaria, and T.A. Khalifa, On Effect of FSP on Microstructural and Mechanical Characteristics of A390 Hypereutectic Al-Si Alloy, *Mater. Sci. Technol.*, 2010, **26**(9), p 1120–1124